Frontiers in Mechanochemistry and Mechanical Alloying

INCOME2008
1-4 December, 2008

MECHANOCHEMICAL SYNTHESIS, CHARACTERIZATION AND PHOTOCATALYTIC PROPERTIES OF M_2O_3/TiO_2 (M = Fe, Mn) NANO-COMPOSITE UNDER VISIBLE LIGHT

Tanmay K Ghorai[1,2], Panchanan Pramanik [1, ξ]
[1]Department of Chemistry, Indian Institute of Technology Kharagpur
Kharagpur-721302, India
[2]Department of Chemistry, Bajkul Milani Mahavidyalaya,
Kismat Bajkul, Purba Medinipur-721655, India

Keywords: Solid solution; M_2O_3/TiO_2 (M = Fe, Mn); Nanocatalysts; Photodegradation

Abstract

Nano-particles of homogeneous solution between TiO_2 and M_2O_3 (M = Fe, Mn; upto 10 wt %) have been prepared by mechanochemical milling of TiO_2 and yellow/Red Fe_2O_3 and Mn_2O_3 using a planetary ball mill. Photocatalytic activities of TiO_2 / M_2O_3 powders were investigated by photooxidation of different dyes like Rhodamine B (RB), Methyl orange (MO), thymol blue (TB) and Bromocresol green (BG) under visible light (300-W Xe lamp; $\lambda > 420$ nm). The results show that the alloy of TiO_2 with 5 wt % of Fe_2O_3 (YFT1) exhibit photocatalytic activity 3-5 times higher than that of P25 TiO_2 and 5 wt % of Mn_2O_3 /TiO_2 (MNT1). Therefore, we have mainly discussed on Fe_2O_3/TiO_2 alloy. XRD of powders show that it has anatase structure with no peak of any of Fe_2O_3/Mn_2O_3. EDX spectra show that Fe/Mn is uniformly distributed in TiO_2. The average particle size and crystallite size of YFT1, MNT1 were found to be 30±5 nm (TEM), 100±5 nm (SEM) and 12 nm (XRD) respectively. Optical adsorption edge of YFT1 is found to be 2.26 eV. EPR and magnetic susceptibility show that Fe^{3+} is in low spin state corresponding to μ_B = 1.8 BM. As the band edge is lower than TiO_2, which means that Fe^{3+} is situated in between conduction band and valence band. The optical absorption causes the formation of hole on Fe^{3+} and liberated electron goes to conduction band. This charge separation is facilitated by visible light rather than UV or near UV light due to lesser energy gap between Fe^{3+} and bottom of conduction band. The oxidation state of iron has been found to be +3 from redox titration and XPS.

Introduction

The photocatalytic oxidation of organic and inorganic compounds is very promising for the purification of industrial wastewater and thus has attracted extensive attention during these 20 years. Due to its stability, non-toxicity and low cost, TiO_2 has been the most investigated photocatalyst for the removal of organic pollutants from water or air [1-10]. The band gap of this semiconductor is 3.2 eV, which corresponds to radiation wavelength of around 380 nm; therefore, a UV light with wavelength shorter than 380 nm is needed to excite electrons in valence band to conduction band. The electron-hole pairs thus generated serve as the oxidizing and reducing agents [6, 10].

The photocatalytic property of a multicomponent system is strongly influenced by the composition, preparation procedure, dynamics of charge transfer, trapping and recombination, and photocatalytic behavior. In recent years, the application of heterogeneous photocatalysis on the removal of contaminants in air and wastewater has fetched some interest [11-15].

However, TiO_2 follows a relatively high electron-hole recombination rate, which is detrimental to its photoactivity. The doping of TiO_2 with transition metal ions like Ni (II) [16], Cu (II) [17], Nb (V) [18], Cr (III) [19-20], Fe (III) [21-24], Mn (II) [25] and metal molybdates [13] were reported to improve the photocatalytic properties with enhanced absorption of visible/ultraviolet light. Binary metal oxides such as TiO_2/WO_3, TiO_2/MoO_3, TiO_2/SiO_2 and TiO_2/ZrO_2 have been widely studied for their unique chemical, physical and photocatalytic properties [26-29]. Studies with a $Fe_2O_3/SrTiO_3$ mixed oxide photocatalyst have shown improved photocatalytic activity for photo-oxidizing methanol under visible light irradiation [30]. Adel Ali Ismail has prepared the ternary heterogeneous mixed oxides i.e. $Y_2O_3/Fe_2O_3/TiO_2$ nanoparticles [31], showed better photooxidation for EDTA than pure TiO_2. Recently, Fe_2O_3/TiO_2 and $MnOx/TiO_2$ heterogeneous mixed oxides [32-37] have shown better photocatalytic activity than pure TiO_2 for oxidation of different organic compounds such as methylene blue, chloroform, formaldehyde, indigo carmine dye, and NO reduction respectively, but these catalysts are inferior to Degussa P 25.

In this study a homogeneous solution between Fe_2O_3 and TiO_2 has been made by high energy mechanical milling using various source of Fe^{3+} which shows high photochemical activity than other prepared photocatalyst (TiO_2 and M_2O_3 (M = Fe, Mn; upto 10 wt %) and it was more active than Degussa P 25 in visible light for oxidative degradation of various dyes. This is observed that the photocatalytic activity of Fe-Ti oxides alloy largely depends on iron content, preparative condition and sintering temperature having optical adsorption edge around 2.2 eV, which facilitates a strong absorption of visible light. The Fe_2O_3/TiO_2 alloys in different mole ratio were prepared by mechanical milling method (using a ball mill) and their photocatalytic activities were evaluated by the photooxidations of different dyes like Rhodamine B (RB), Methyl orange (MO), thymol blue (TB) and Bromocresol green (BG) under visible light (300-W Xe lamp; $\lambda >$ 420 nm) irradiation. The alloy of Fe_2O_3 (5 wt. %) with TiO_2 (anatase) is better photoactive compared to Degussa P25 TiO_2 and other compositions of M_2O_3/TiO_2 (M = Fe, Mn).

ξ email : panchanan_123@yahoo.com

Experimental

Synthesis of M_2O_3 /TiO_2 (M = Fe, Mn) Photocatalysts

A stoichiometric mixture of TiO_2 (Aldrich, 99.99%) and M_2O_3 (M = Fe and Mn) with different wt % (metal ions in TiO_2 is 5, 7 and 10 wt %) was prepared by mechanical grinding in a planetary ball mill using small amount of water for iron and ethanol for Mn system. The sources of Fe^{3+} were yellow/red iron oxide (99.9 %, Tata-Pigment, India) and precipitated ferric hydroxide and Mn^{2+} from potassium permanganate (Aldrich, 99.99%). The mechanical milling was allowed for 4 hours for complete mixing the oxides and forming a solid solution. The milling was performed in Fritsch Pulverisette No. 6 planetary ball mill, using a rotational speed of 250 rpm at a constant rotation direction and a ball to powder weight ratio of 10:1. Both the container and balls were made of aluminium oxide. The prepared samples were dried at 100 ^oC for 15 h in an oven and photocatalytic activity was studied. The heat-treatment of the sample at a temperature higher than 200 ^oC had poor photocatalytic activity. Rhodamine B (RB), Methyl orange (MO), Thylmol blue (TB) and Bromocresol green (BG) were of AR grade and procured from MERCK, India.

Photocatalytic Experiment

Photocatalytic experiments were conducted using nano-photocatalysts in presence of photocatalytically degradable different dyes in water solution. The photocatalytic reaction was carried out under visible light irradiation with slow stirring (using magnetic stirrer) of the solution mixture and M_2O_3/TiO_2 (M = Fe, Mn) photocatalysts. The light source was a 300-W Xe lamp (ILC technology; CERMAX LX-300F). The container was Petridis of volume 200ml. The reactions were performed by adding nano powder of each photocatalyst (0.1 g) into each set of a 100 ml of different solution of dyes.

Analytical Methods

A small volume (1ml) of reactant liquid was siphoned out at regular interval of time for analysis. It was then centrifuged at 1100 rpm for 15 min, filtered through a 0.2µm-millipore filter to remove the suspended catalyst particles and concentration of dye was measured by absorption spectrometry using UV-VIS spectrometer (UV-1601, SHIMADZU) at its wavelength of maximum absorption.

Characterization

The crystal structure of the prepared samples was determined by the X-ray diffractometer (XRD) (Model: Philips PW 1710) equipped with a Cu Kα radiation. The accelerating voltage and current used were 40 kV and 20 mA, respectively. The 2θ ranged from 15 to 70 °. Crystallite sizes (D) of the obtained powders were calculated by the X-ray line broadening technique performed on the direction of lattice using computer software (APD 1800, Philips Research Laboratories) based on Scherer's formula [38] :

$$D = \frac{0.89\lambda}{\beta \cos\theta} \quad (1)$$

where D is the Crystallite size, λ is the X-ray wavelength, θ is the Bragg's angle and β is half width.

The stoichiometry of M_2O_3/TiO_2 (M = Fe, Mn) alloys have been examined by energy dispersive X-ray spectroscopy (EDX) (JEOL JMS-5800) which is consistent with the amount of M_2O_3 (M = Fe and Mn) and TiO_2 taken during synthesis. The FT-IR analysis was performed using a Perkin-Elmer Paragon 1000 FT-IR spectrometer and BET surface area measurements were carried out using a BECKMAN COULTER SA3100 through nitrogen adsorption-desorption isotherm at 77K. X-ray photoelectron spectroscopy (XPS) measurements were carried out in an Axis-Ultra X-ray photoelectron spectrophotometer in vacuum (1×10^{-5} Pa).

The UV–VIS diffuse reflectance spectra of the prepared powders were obtained by a UV–VIS spectrophotometer (UV-1601 Shimadzu) at room temperature. The average sizes of nanoparticles were measured in the transmission electron microscopy (TEM) (Model Philips TM-30, Philips Research Laboratories). The magnetic susceptibility was measured by Guoy balance. The ESR spectrum was obtained by BURCKER ER083CS model at room temperature (ca. 298 K).

Results and Discussion

XRD Analysis

Figure 1 shows the XRD patterns of YFT1, YFT2, YFT3, RFT1, RFT2, MNT1, TiO_2, and YF/RF (abbreviation presented in Table 1) mixed oxides nanopowders heat treatment at 100 ^oC for 15 h in air atmosphere. It has been observed that the phases prepared at different wt % of mixed oxides TiO_2 and M_2O_3 (M = Fe and Mn) (YFT1, YFT2, YFT3, RFT1, RFT2 and MNT1) have anatase phase upto 5 wt % of Fe_2O_3/Mn_2O_3 (as per JCPDS No. 84-1285), and YF/RF (have same XRD) are hexagonal phases (as per JCPDS No. 86-0550). The XRD pattern of TiO_2 sample shows distinct peaks of the anatase phases, without any indication of rutile phases. XRD of YFT1, YFT2, RFT1, RFT2 and MNT1 indicates no change of crystallographic characteristics, which is shown in Fig. 1. XRD also indicates that the final products after ball milling have anatase phase of TiO_2 and Fe ions are well inserted into the framework of the TiO_2 anatase structure upto certain wt % (5 wt%) of alloy, after that increse the Fe concentrations and iron peaks appears on the XRD of YFT3. Among all the mixed oxides TiO_2 with M_2O_3 (M = Fe and Mn), only Fe_2O_3/TiO_2 (YFT1) is reasonably photoactive (shown in Fig. 8) compare the other prepared photocatalyst, against RB solution, for which we have concentrated our discussion mainly on Fe_2O_3/TiO_2 (iron oxide in TiO_2 is 5, 7 and 10 wt %) catalyst. The small incorporation of Fe^{3+} in TiO_2 will not change much of the XRD peaks. The change will be in first or second decimal of theta value, because ionic radius of Ti^{4+} and Fe^{3+} are very close (60.5 and 55 pm). More over magnetic data and EPR data does not infer any aggregation of Fe^{3+} as Fe_2O_3 crystal. Due to broad peaks of XRD we are unable to evaluate the accurate d-values of lattices. After photochemical reaction, no metal ion leaching was observed. The sample prepared with red Fe_2O_3 and yellow Fe_2O_3 or precipitated $Fe(OH)_3$ gave same chemical and physical characteristics. Average crystallite sizes of the prepared photocatalysts were calculated according to Scherer's formula and indicated that the crystallite sizes of the samples were approximately 12-15 nm. The atomic level dispersion Fe_2O_3/TiO_2 and Mn_2O_3/TiO_2 have been presented in Fig. 2 (A) and Fig. 2 (B) through energy dispersive X-ray spectroscopy. The Al peaks comes in the EDX spectra due to instrumentation error.

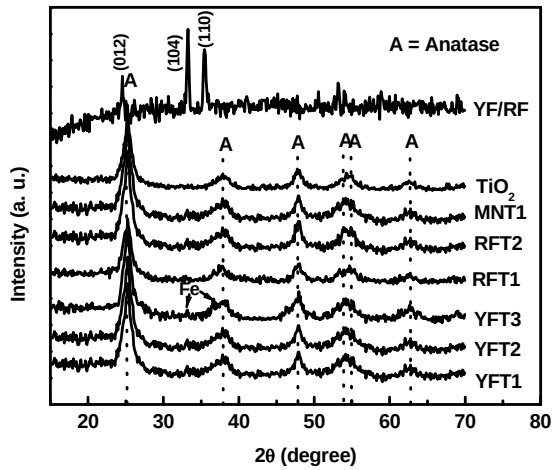

Figure 1. A comparison of X-ray diffraction patterns of YFT1, YFT2, YFT3, RFT1, MNT1, TiO_2, YF and RF nanopowders prepared by mechanochemical method after heat treatment at 100 ^oC for 15 h

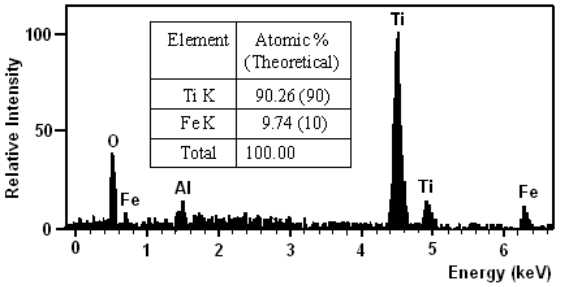

(A)

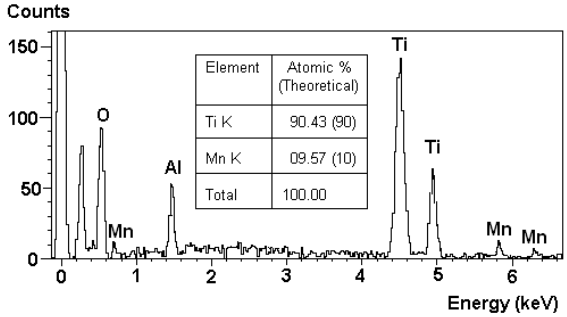

(B)

Figure 2. (A) EDX spectra of Fe_2O_3 (5 wt %) /TiO_2 (YFT1), 2 (B) EDAX of Mn_2O_3 (5 wt %)/TiO_2 (MNT1)

Specific Surface Area (BET) Analysis

The BET surface area of Fe_2O_3/TiO_2 composite powders (YFT1) calcined at 100 ^oC was 58.5 m^2/g, while the surface area of P25 is 49.1m^2/g and the surface area of other prepared photocatalysts are presented in Table 1. Though surface area of YFT1, RFT1, MNT1 and Degussa P25 are comparable, but photocatalytic activity of YFT1/RFT1 is few times greater than P25 and MNT1. Therefore, among all the prepared photocatalyst the YFT1/RFT1 is more photoactive for faster degradation of different dyes like RB, MO, TB and BG under visible light (300-W Xe lamp; λ>420 nm).

Transmission Electron Microscopy (TEM) Analysis

Nanoparticles with average size about 30±5 nm were observed in the transmission electron microscopy (TEM) of YFT1. This has been shown in Fig. 3. The calculated crystallite size of YFT was about 12-13 nm obtained from XRD (shown in Table 1).

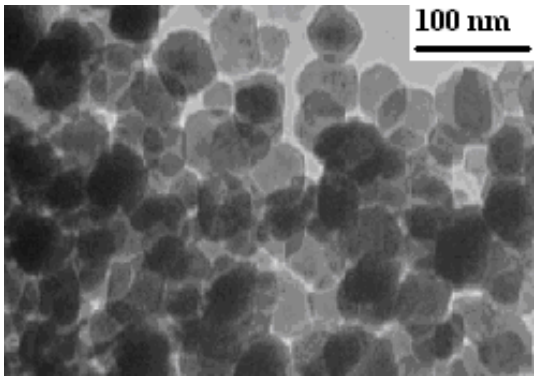

Figure 3. TEM micrograph of YFT1

Table 1. Resultant properties of YFT1, YFT2, YFT3, RFT1, RFT2, MNT1, FT, P25, YF and RF composites

Acronym*	S_{BET} (m^2/g)	Anatase crystal size (nm)	Absorption edge (nm)	Effective Band gap Energy (eV) (from optical spectra)
YFT1	58.5	12.17	548	2.26
YFT2	52.2	12.38	520	2.38
YFT3	48.6	12.43	508	2.48
RFT1	55.2	12.35	540	2.29
RFT2	50.3	12.63	470	2.63
MNT1	36.6	12.22	-	-
FT	56.6	12.22	548	2.26
P25	49.1	12.46	387	3.20
YF	4.8	20.05	563	2.20
RF	4.1	21.26	558	2.23

* Acronym

YFT1 Yellow Fe_2O_3 (5 wt %)/TiO_2 FT $Fe(OH)_3$(5wt %) /TiO_2
YFT2 Yellow Fe_2O_3 (7 wt %)/TiO_2 P25 Degussa P25
YFT3 Yellow Fe_2O_3 (10 wt %)/TiO_2 YF Yellow Fe_2O_3
RFT1 Red Fe_2O_3 (5 wt %)/TiO_2 RF Red Fe_2O_3
RFT2 Red Fe_2O_3 (7 wt %)/TiO_2
MNT1 Mn_2O_3 (5 wt %)/TiO_2

BET surface area measured by dinitrogen adsorption desorption isotherm at 77K

FT-IR Spectra Analysis

FT-IR spectra shown spectrum of YFT1, and RFT1 are similar to TiO_2 but MNT1is tiny different, shown in Fig. 4. This indirectly indicates that Fe_2O_3 has been dissolved into the TiO_2 lattices. The two bands observed at about 3400 and 1600 cm^{-1} are characteristic of the H–O bending mode of hydroxyl groups present on the surface due to moisture. These are crucial to the photocatalytic reactions since they can react with photoexcited holes generated on the catalyst surface and produce hydroxyl radicals [39], which are powerful oxidant. The absorption band around 463 cm^{-1} and

1200 cm^{-1} may be assigned to the Ti–O–Ti bending [33]. The absorption band at 609 cm^{-1} attributes to the Ti–O stretching vibrations of TiO_2 anatase phase and their small peaks around 1405 and 1051 cm^{-1} of samples YFT1, RFT1 and YFT4 were detected. There were no eminent peaks of undissolved Fe_2O_3. This indirectly indicates that Fe_2O_3 has been dissolved into the TiO_2 lattices and form solid solution. The new peaks (1405 and 1051 cm^{-1}) may assigned to Ti-O-Fe hetero bond. In fact, a vibration frequency reduction would indicate a higher ionization of the metallic atom on which the molecule is adsorbed. The band at 1405 cm^{-1} is attributed to adsorbed dyes on Fe atoms and 1051 cm^{-1} attribute to carbonates. The presence of carbonate vibrations can be well resolved in all metastable alloy samples as shown in Fig. 4. The alloys on heating above 600 ^oC segregate the pure phases of TiO_2 and Fe_2O_3. It shows that the alloys have metastable phases between TiO_2 and Fe_2O_3.

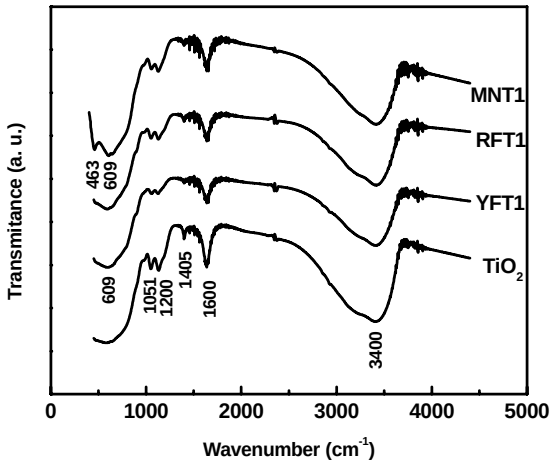

Figure 4. FT-IR spectra for YFT1, RFT1, MNT1 and TiO_2 samples

EPR Spectrum Study

From electronic paramagnetic resonance spectrum (EPR) of YFT1 and MNT1 shown in Fig. 5(A) and Fig. 5(B) respectively, reflected a signal at a g-tensor value of 1.991 in both cases. The Fig. 5 (A) indicated the presence of low spin state of Fe^{3+} in TiO_2 [40]. Due to absence of any hyperfine line in ESR spectra, it can be suggested that Fe^{3+} cations are well separated. But Fig. 5 (B) show high spin state of Mn^{3+} in TiO_2 due to five-line multiplet spectrum which results from the hyperfine interaction of the $^5D_0$ ground state with the Mn nucleus (I = 2). No EPR signal was detected on pure TiO_2. The magnetic moment of YFT1/RFT1 is found to be 1.73 BM measured by Guoy's Method. It indicates that the Fe^{3+} in YFT1/RFT1 alloy contains one unpaired electron. This infers that iron exists as a Fe^{3+} ion in the system under strong crystal field environment producing low spin Fe^{3+}. The magnetic moment does not change reasonably with lowering temperature which indicates that Fe-Fe spin interaction is absent (Fig. 6) at 5 wt.% of Fe_2O_3. Such type of magnetic moment data is not observed in MNT1 system.

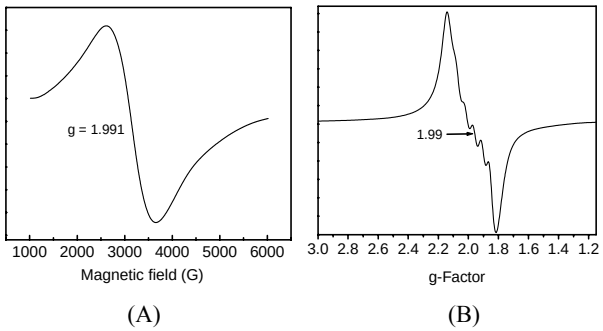

Figure 5. (A) EPR spectrum of YFT1, (B) EPR spectrum of MNT1

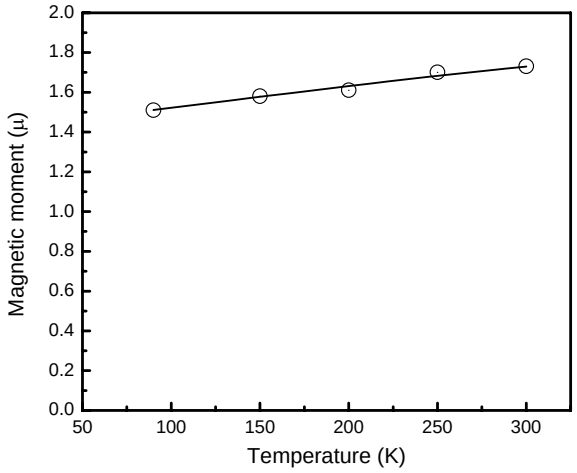

Figure 6. Magnetic susceptibility measurement of YFT

Oxidation States of Fe Ion (XPS Study)

The oxidation state of Fe^{3+} have been determined by redox titration and XPS. Known amount of catalyst is treated with HF and KBr in absence of air (under argon atmosphere and was back titrated with Mohr salt solution (Fe^{2+}). No Fe^{2+} of Mohr salt solution was consumed in the titration. This indicates the absence of any higher oxidation states (4+ / 5+ /6+) of Fe. Any higher oxidation of Fe could liberate Br_2 and would have been consumed by Fe^{2+}. Figure 7 shows the XPS spectra of Fe_2O_3/TiO_2. XPS has shown the only peak of Fe^{3+}. The photoelectron peaks at 710.8 eV and 724.7 eV in Fig. 7 were corresponding to binding energy of $Fe2p_{3/2}$ and $Fe2p_{1/2}$ of Fe^{3+}, consistent with the values reported in literature [41]. The photoelectron peaks of Ti is observed but not shown in the figure. The surface atomic concentration of the Fe_2O_3 (5 wt%)/TiO_2 alloy estimated from XPS was shown in Table 2. The surface atom concentrations for oxygen, titanium and iron atoms and the atomic ratio for Fe/Ti (10.24) (the atomic ratio is also matched with EDX data) were obtained from the results of XPS analysis. The oxidation state of Mn in MNT1 is +3 also observed from XPS.

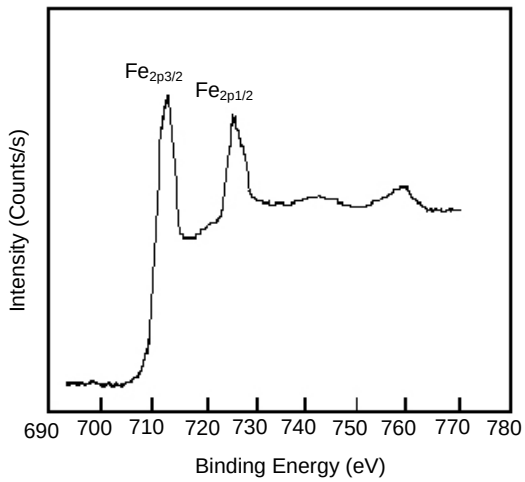

Figure 7. XPS spectrum of Fe_2O_3/TiO_2

Table 2. The surface atom concentration for oxygen, Fe and Ti atoms of the Fe_2O_3 (5 wt %)/TiO_2 alloys by XPS

Sample	Atomic Surface concentration (%)			Surface atomic ratio (%)
	O	Ti	Fe	Fe/Ti
Fe_2O_3 (5 mol%)/TiO_2	67.29	29.67	3.04	10.24

Photocatalytic Activity of the Prepared Samples

The photooxidation of different coloured dyes solution like RB, MO, TB and BG to colourless solution under prepared photocatalysts and visible light (300-W Xe lamp; λ>420 nm) irradiation was shown in Fig. 8, 9, 10 and 11 respectively. UV–VIS spectra of RB, MO, TB and BG taken after the irradiation with M_2O_3/TiO_2 (M = Fe and Mn) compositions (YFT1, YFT2, YFT3, RFT1, RFT2, MNT1, P25, YF and RF) were measured and corresponding absorbance of dyes were found at 554, 464, 597 and 616 nm respectively. Time required for complete degradation of different dyes were found to be about 60 min for RB, 90 min for MO, 105 min for TB, and 150 min for BG in presence of YFT1 catalyst. Comparatively the rate of degradation of Rhodamine B is faster among all the four dyes. For all the cases the catalysts were taken 1 g/l and different dyes concentration was about in 10 mM. The photocatalytic activities have presented in Fig. 8, 9, 10 and 11. Under visible light irradiation, the alloy YFT1/RFT1 powder exhibited highest photocatalytic activity than that of other compositions of M_2O_3/TiO_2 (M = Fe and Mn) mixed oxides, P25 TiO_2, MNT1, and pure yellow/red Fe_2O_3 for all the four dyes solutions. It is also observed that in absence of catalyst the degradation of dyes is not possible under visible light (shown in Fig, 8, 9, 10 and 11). The YFT1/RFT1 alloy powders have shown five times higher photocatalytic activity than that of P25 in case of Rhodamine B and three times higher photoactivity than that of P25 in case of other three dyes (MO, TB and BG). The increment of Fe_2O_3 concentration beyond 5 wt % leaded lower photocatalytic activity. The degradation rate constant (*k*) for RB, MO, TB and BG using YFT1, YFT2, YFT3, RFT1, RFT2, MNT1, P25, YF and RF photocatalysts have been presented as the time required for 50 % decolourization of dyes solutions in Table 3. The photocatalytic activity is independent of source of Fe^{3+}. The source may be yellow oxide or red-oxide.

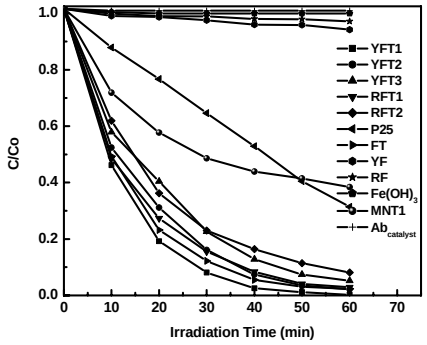

Figure 8. The Rhodamine B oxidation in UV-vis absorption spectra at 554 nm as a function of visible light irradiation time in the prepared photocatalysts calcined at 100 ºC for 15 h, and absence of catalyst ($Ab_{catalyst}$), 300-W Xe lamp with a cutoff filter (λ > 420 nm)

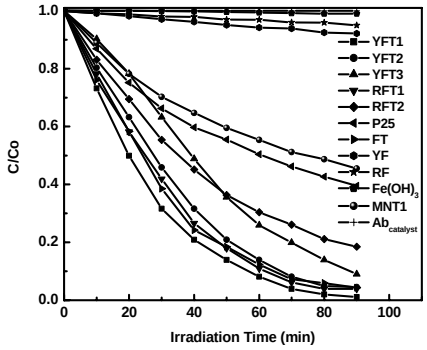

Figure 9. The methyl orange oxidation in UV-vis absorption spectra at 464 nm as a function of visible light irradiation time in the prepared photocatalysts calcined at 100 ºC for 15 h, and absence of catalyst ($Ab_{catalyst}$), 300-W Xe lamp with a cutoff filter (λ > 420 nm)

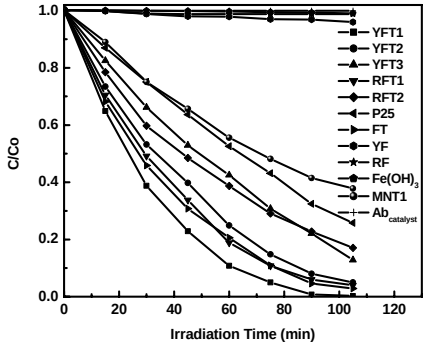

Figure 10. The thymol blue oxidation in UV-vis absorption spectra at 597 nm as a function of visible light irradiation time in the prepared photocatalysts calcined at 100 ºC for 15 h, and absence of catalyst ($Ab_{catalyst}$), 300-W Xe lamp with a cutoff filter (λ > 420 nm)

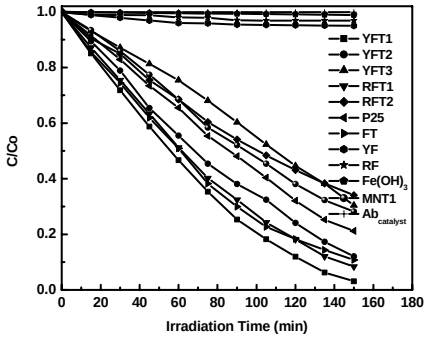

Figure 11. The Bromocresol green oxidation in UV-vis absorption spectra at 616 nm as a function of visible light irradiation time in the prepared photocatalysts calcined at 100ºC for 15 h, and absence of catalyst ($Ab_{catalyst}$), 300-W Xe lamp with a cutoff filter ($\lambda > 420$ nm)

Table 3. Degradation rate constants of different organic dyes in different pH using different photocatalysts of YFT1, YFT2, YFT3, RFT1, RFT2, MNT1, FT, P25, YF and RF

Photocatalysts	Reaction rate constant k ($x10^{-3}$ min^{-1})			
	Dye (pH)			
	RB (7.01)	MO (6.99)	TB (8.01)	BG (8.03)
YFT1	84.30	39.44	37.12	13.87
YFT2	61.40	31.28	23.20	10.51
YFT3	50.10	20.63	14.29	5.10
RFT1	62.67	34.38	27.80	12.13
RFT2	49.51	20.2	15.85	6.70
MNT1	24.58	10.36	9.81	8.13
FT	70.65	33.83	26.36	12.81
P25	15.09	11.75	10.74	7.86
YF	1.33	0.98	0.38	0.54
RF	0.89	0.58	0.23	0.26

RB; Rhodamine B, MO; Methyl Orange, TB; Thymol Blue, BG; Bromocresol Green

The concentration of the different dyes is ~ 10 mM

The catalyst concentration is $C_{catalysts}$ = 1 g/l. Time required for 50% decolorization of different organic dyes solution

All photocatalysts are calcined at 100 ˚C for 15 h

UV-VIS Diffuse Reflectance Spectrum

The UV-VIS diffuse reflectance spectrum of alloys of Fe_2O_3/TiO_2 and pure TiO_2 have been presented in Fig 12. It has reflected distinct absorption edges at 548 nm, 540 nm, nm, 520 nm, 508 nm, 470 nm, 563 nm, 558 nm and 387 nm for YFT1, RFT1, YFT2, YFT3, RFT2, YF, RF and pure TiO_2 respectively and corresponding band edge energies are 2.26, 2.29, 2.38, 2.44, 2.63, 2.2, 2.22 and 3.20 eV respectively presented in Table 1. With increase of Fe^{3+}, the band end edge position shifted to slightly higher energy value possibly due to more inclusion of defect structures. With increasing the dopant concentration, the band edge energy increases, as a consequence the photocatalytic activity decreases. This may be assigned to the absorption edge increases to higher wave length, then it cover more frequency and transition probability at higher frequency will be more (it easily understood from the spectra). This causes the increase of efficiency. YFT1 photocatalysts has lower band gap energy (2.26 eV) with highest photocatalytic activity compared to other Fe_2O_3/TiO_2 alloys and P25. Further decrease of concentration of Fe^{3+} may decrease the band edge but it may reduce kinetics of reaction resulting in lower photo-catalytic activity.

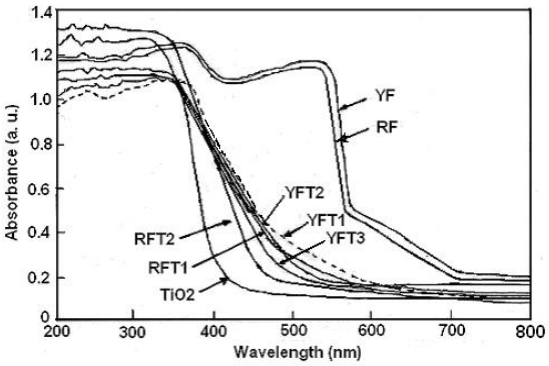

Figure 12. UV-vis diffuse reflectance spectra of synthesized YFT1, YFT2, YFT3, RFT1, RFT2, RFT3, TiO_2, YF and RF powders

Tentative Mechanism of Photosensitization of Fe_2O_3/TiO_2 (YFT/RFT) under Visible Light Irradiation

The tentative mechanism of photooxidation may be as follow. Fe^{3+} ion on absorption light produces Fe^{4+} and excited electron. This electron is promoted to conduction band (CB). The exited electron is trapped in CB through the formation $O_2^{\cdot -}$ using O_2 from the atmosphere on the surface. On the other side the dye is sensitized and the dye cation is formed by using irradiation of visible light of >420 nm. The dye cation is unstable and decomposes with react with TiO_2/Fe_2O_3 (Fe^{4+}) through the production of highly oxidative radical species such as super oxide radical anion O_2^{-} on the surface of the catalyst. The Fe^{4+} initiates the oxidative degradation of organic compounds further assisted by super oxide radical. We tried to identify the formation of Fe^{4+} through ESR spectra under illumination. Due opacity of the sample we could not get any well resolved spectra. The Schematic diagram of reaction mechanism is presented in Fig. 13.

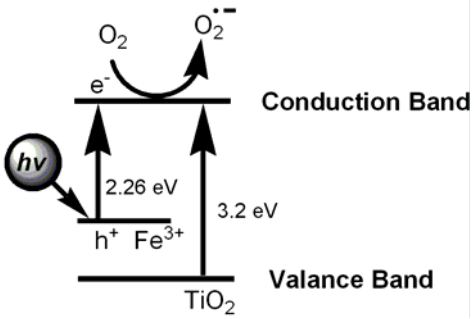

Figure 13. Tentative Schematic diagram of reaction mechanism of YFT photocatalysts under visible light irradiation

Conclusions

Synthesis of nano-sized homogeneous solid solution between Fe_2O_3 and TiO_2 with high photocatalytic activity for oxidative degradation of dyes was successfully obtained through mechanochemical synthesis. The activity is better than P-25. The main observations are:

1. XRD data shows the formation of solid solution having anatase structure with no free Fe_2O_3 upto 5 wt % of Fe_2O_3. The chemical and physical natures of the materials remain same irrespective of the source of Fe_2O_3.
2. Fe_2O_3/TiO_2 catalyst have crystallite size about 12-13 nm (measured from XRD) and particle size about 30±5 nm (measured from TEM).
3. FT-IR of YFT1, RFT1 and MNT1 are similar to pure TiO_2. This indicates that Fe_2O_3 is dissolved into the TiO_2 lattices.
4. The maximum solubility of Fe_2O_3 in TiO_2 is 5 wt % of Fe_2O_3 irrespective of source and this composition has highest photocatalytic activity.
5. Catalyst with 5 wt % of Fe_2O_3 exhibited photocatalytic activity 3-5 times higher than P25 TiO_2 and MNT1 for the oxidation of different dyes. Rate of degradation of Rhodamine B is faster among all the four dyes.

Acknowledgements

This work was supported by the Council of Scientific and Industrial Research, India. The authors are grateful for its financial support.

References

1. L Körösi, A. Oszkó, G.Galbács, A. Richardt, V. Zöllmer, I. Dékány, *J. Appl. Catal. B. Environ.* 77 (1-2) (2007)175-183.
2. L. Korösi, Sz. Papp, I. Bertóti, I. Dékány, *Chem. Mater*, 19 (19) (2007) 4811-1819.
3. P. Calza, E. Pelizzetti, K. Mogyorósi, R. Kun, I. Dékány, *J. Appl. Catal. B. Environ.,* 72 (2007) 314-321.
4. L. Korösi, I. Dékány, *Colloids and Surfaces A*, 280 (2006)146-154.
5. Y. Yang, X-jun Li, J-tao Chen, L-yan Wang, *J. Photochem. Photobiol. A: Chem.,* 163 (2004) 517-522.
6. M. R. Hoffmann, S. T. Martin, W. Choi, D. W. Bahnemann, *Chem. Rev.,* 95 (1995) 69.
7. L A. Linsebigler, G. Lu, Jr. J. T. Yates, *Chem. Rev.,* 95 (1995) 735.
8. M. Janus, A. W. Morawski, *Appl. Catal. B: Environ.,* 75 (2007) 118-123.
9. V. Stengl, S. Bakardjieva, N. Murafa, J. Subrt, H. Mestankova , J. Jirkovsky, *Mater. Chem. Phys.,* 105 (2007) 38-46.
10. I. K. Konstantinou, T. A. Albanis, *Appl. Catal. B: Environ.,* 49 (2004) 1-14.
11. D. Beydoun, H. Tse, R. Amal, G. Low, S. McEvoy, *J. Mol. Catal. A: Chem.*, 177 (2002) 265-272.
12. T. Ohno, K. Sarukawa, M. Matsumura, *J. Phys. Chem. B,* 105 (2001) 2417-2420.
13. T. K. Ghorai, D. Dhak, S. K. Biswas, S. Dalai, P. Pramanik, *J. Mol. Catal. A: Chem.,* 273 (2007) 224-229.
14. J-Chuan Xu, Y-Li Shi, J-Er Huang, B. Wang, H-Lin Li, *J. Mol. Catal. A: Chem.,* 219 (2004) 351-355.
15. M. A. Hasnat, M. M. Uddin, A. J. F. Samed, S. S. Alam, S. Hossain, *J. Hazardous Mater.,* 147 (2007) 471-477.
16. D. Jing, Y. Zhang, L. Guo, *Chem. Phys. Lett.,* 415 (2005) 74-78.
17. G. Colon, M. Maicu, M. C. Hidalgo, J. A. Navio, *Appl. Catal. B: Environ.,* 67 (2006) 41-51.
18. K. Tennakone, J. Bandara, *Sol. Energy Mater. Sol. Cells,* 60 (2000) 361.
19. N. Serpone, D. Lawless, *Langmuir,* 10 (1994) 643.
20. J. C. Yu, G. Li, X. Wang, X. Hu, C. W. Leung, Z. Zhang, *Chem. Commun.,* (2006) 2717–2719.
21. J. Zhu, W. Zheng, B. He, J. Zhang, M. Anpo, *J. Mol. Catal. A: Chem*., 216 (2004) 35-43.
22. Z. Zhang, C. Wang, R. Zakria, J. Y. Ying, *J. Phys. Chem. B,* 102 (1998) 10871-10878.
23. M. I. Litter, J. A. Navio, *J. Photochem. Photobiol. A: Chem.,* 98 (1996) 171-181.
24. J. Feng, R. S. K. Wong, X. Hu, P. L. Yue, *Catal. Today,* 98 (2004) 441-446.
25. R. Arroyo, G. Cordoba, J. Padilla, V. H. Lara, *Mater. Lett.,* 54 (2002) 397.
26. Y. R. Do, W. Lee, K. Dwight, A. Wold, *J. Solid State Chem.,* 108 (1994) 198.
27. J. Papp, S. Soled, K. Dwight, A. Wold, *Chem. Mater.,* 6 (1994) 496.
28. X. Fu, L. A. Clark, Q. Yang, M. A. Anderson, *Environ. Sci. Tech.,* 30 (1996) 647.
29. Z. Liu, J. Davis, *J. Phys. Chem.,* 98 (1994) 1253.
30. H. Zhang, X. Wu, Y. Wang, X. Chen, Z. Li, T. Yu, J. Ye, Z. Zou, *J. Phys. Chem. Solids,* 68 (2007) 280-283.
31. A. A. Ismail, *Appl. Catal. B: Environ.,* 58 (2005) 115-121.
32. E. Celik, A. Y. Yildiz, N. F. Ak Azem, M. Tanoglu, M. Toparli, O.F. Emrullahoglu, I. Ozdemir, *Mater. Sci. Eng. B,* 129 (2006) 193-199.
33. M. Kang, Suk-Jin Choung, J. Y. Park, *Catal. Today,* 87 (2003) 87-97.
34. J. Yang, D. Li, Z. Zhang, Q. Li, H. Wang, *J. Photochem. Photobiol. A: Chem.,* 137 (2000) 197-202.
35. L. Diamandescu, M. Feder, D. Tarabasanu-Mihaila, F. Vasiliu, *Appl. Catal. A: Gen.,* 325 (2007) 270–275.
36. M. M. Mohamed, I. Othman, R. M. Mohamed, *J. Photochem. Photobiol. A: Chem.,* 191 (2007) 153–161.
37. J. Li, J. Chen, R. Ke, C. Luo, J. Hao, *Catal. Commun.,* 8 (2007) 1896–1900.
38. P. Klug, L. E. Alexander, Direction Procedures for Polycrystalline and Amorphous Materials, Wiley, New York, 1954.
39. Z. Ding, G. Q. Lu, P. F. Greenfield, *J. Phys. Chem. B* 104 (2000) 4815.
40. C. Adan, A. Bahamonde, M. Fernandez-Garcia, A. Martinez-Arias, *Appl. Catal. B: Environ.* 172 (2007) 11-17.
41. Z. Yuan, J. Zhang, B. Li, J. Li, *Thin Solid Films* 515 (2007) 7091–7095.